J Appl Electrochem (2012) 42:961–968
DOI 10.1007/s10800-012-0463-8

ORIGINAL PAPER

Electrochemical behavior and electrodeposition of dysprosium in ionic liquids based on phosphonium cations

Akifumi Kurachi · Masahiko Matsumiya · Katsuhiko Tsunashima · Shun Kodama

Received: 8 May 2012 / Accepted: 22 July 2012 / Published online: 4 August 2012

Abstract The electrochemical behavior and the electrodeposition of dysprosium (Dy) in phosphonium-cation-based ionic liquid were investigated in this study. A new group of the room-temperature ionic liquids (RTILs) based on phosphonium cations with bis(trifluoromethylsulfonyl)amide anions was applied as novel electrolytic solutions. The cyclic voltammetric measurements resulted in one step reduction of the trivalent dysprosium ion in phosphonium-cation-based ionic liquid. On the other hand, no anodic peak ascribed to the oxidation of dysprosium metal was observed in this electroanalytical study. The diffusion coefficient and the activation energy for diffusion of the trivalent Dy complex in IL were estimated using semi-integral analysis, because it is important to analyze the diffusion properties to recover Dy through electrowinning methods. The diffusion coefficient of Dy(III) which was calculated to be 2.0×10^{-12} m^2 s^{-1} at 25 °C, closed to that of the trivalent lanthanoid ion such as Eu(III) and Sm(III) in phosphonium-cation-based ionic liquid. In addition, the activation energy for diffusion was estimated to be 65 kJ mol^{-1} (0.5 M) and 49 kJ mol^{-1} (0.075 M). The estimated activation energy for diffusion was affected by the concentration of the electrolytic solution, since the RTILs had relatively strong electrostatic interactions between the metal cations and the solvent anions. Furthermore, the electrodeposition of Dy in phosphonium-cation-based IL was carried out using a two-electrode system constructed with a copper plate cathode and dysprosium metal anode. Energy dispersive X-ray analysis of electrodeposits showed a sharply peaked spectrum corresponding to the characteristic X-ray lines of Dy. In addition, the obtained Dy, with the exception of the surface layer, was confirmed to be in the metallic electronic state by X-ray photoelectron spectroscopy.

Keywords Ionic liquids · Phosphonium cations · Diffusion coefficients · Activation energy · Dysprosium · Electrodeposition

Electronic supplementary material The online version of this article (doi:10.1007/s10800-012-0463-8) contains supplementary material, which is available to authorized users.

A. Kurachi (✉)
Department of Electronic Chemistry, Interdisciplinary Graduate School of Science and Engineering, Tokyo Institute of Technology, 4259 Nagatsuta-cho, Midori-ku, Yokohama, Kanagawa 225-8502, Japan
e-mail: kurachi-akifumi-ck@ynu.jp

M. Matsumiya
Graduate School of Environment and Information Sciences, Yokohama National University, 79-2 Tokiwadai, Hodogaya-ku, Yokohama 240-8501, Japan

K. Tsunashima
Department of Materials Science, Wakayama National College of Technology, 77 Noshima, Nada-cho, Gobo, Wakayama 644-0023, Japan

S. Kodama
Nippon Chemical Industrial Co., Ltd, 9-11-1 Kameido, Koto-ku, Tokyo 136-8515, Japan

1 Introduction

Dysprosium (Dy) is a rare-earth element and a lanthanoid. The chemical properties of Dy are similar to those of the other lanthanoids such as cerium, neodymium, europium, ytterbium, etc. Lanthanoids have been widely used recently for plasma display panels [1], inorganic electroluminescent materials [2], rare-earth magnets [3], etc. In addition, Dy is also one of the most important elements for high-tech

industries because it is often used in neodymium magnets as an additive element that prevents them from demagnetizing at high temperature. Neodymium magnets are produced in quantities of more than 30,000 tons/year worldwide as of 2007 [4]. They have been employed as magnetic field sources for magnetic resonance imaging, hard disk drives, and motors for hybrid electric vehicles [3–5]. From the viewpoint of effective use of resources, the recovery of the Dy from neodymium magnets through an electrowinning method will be necessary in the near future, because almost all these magnets are discarded under the present circumstances. However, no such system for recovering Dy using an electrowinning method has developed so far.

Room-temperature ionic liquids (RTILs) composed of bis(trifluoromethylsulfonyl)amide (TFSA) anions are attractive electrolysis solutions for the electrodeposition of electrochemically negative elements because of their high ionic conductivity, wide electrochemical window, thermal stability, noncombustibility, low volatility, chemical stability against moisture, and immiscibility with water [6, 7]. There have been some reports on electrodeposition of metals such as lithium [8] and transition metals [9] using TFSA-based ILs. In addition, TFSA-based ionic liquids (ILs) have been investigated for producing various functional materials such as lithium-ion batteries [10, 11] and for organic electrosynthesis [12]. Various cations can be combined with the TFSA anion, e.g., 1-ethyl-3-methylimidazolium (EMI), 1-*n*-butyl-3-methylimidazolium (BMI), trimethyl-*n*-hexylammonium (TMHA), 1-butyl-1-methylpyrrolidinium (P14), and 1-butyl-1-methylpyrrolidinium (BMP). In this study, we chose a quaternary phosphonium RTIL composed of trimethyl-pentylphosphonium (P_{2225}) cations and the TFSA anion, because this novel IL has better properties than the corresponding ammonium ILs, such as low viscosity, high conductivity, and electrochemical stability [13, 14].

The electrodeposition and electrochemical behavior of Dy in molten salts have already been reported by Massot et al. [15] and Castrillejo et al. [16]. Moreover, Lodermeyer et al. [17] performed electrodeposition of Dy in a non-aqueous electrolyte. Castrillejo et al. reported that Dy(III) is reduced in two steps: $Dy(III) + e^- \rightarrow Dy(II)$, and $Dy(II) + 2e^- \rightarrow Dy(0)$. However, Massot et al. and Lodermeyer et al. reported that the reduction process of Dy(III) proceeded in one step: $Dy(III) + 3e^- \rightarrow Dy(0)$. On the other hand, there has been no investigation of the reduction behavior of Dy in ILs. Thus, the reduction behavior of Dy in molten salts or in ILs has not been revealed so far, and the reduction process of Dy(III) in phosphonium-based ILs needs to be investigated.

As for the reduction behaviors of rare-earth metals, we recently explained that the reduction of rare-earth complexes of europium and samarium [7] proceeded as a quasi-reversible process in phosphonium-based ILs. The electrochemical charge transfer reactions for these complexes were one-electron transfers under diffusion-controlled conditions: $Ln(III) + e^- \rightleftharpoons Ln(II)$ (Ln = Eu and Sm). However, no results were found pertaining to the electrochemical properties and electrodeposition of Dy ions in phosphonium-based ILs. For this purpose, we investigated the electrochemical behavior for Dy(III) in an IL based on phosphonium cations using cyclic voltammetry (CV). In addition, the diffusion coefficients and the activation energy for diffusion of Dy(III) in phosphonium-based IL were estimated using semi-integral analysis (SI). Furthermore, the electrodeposits from the phosphonium-based IL were also investigated by energy dispersive X-ray analysis (EDX) and X-ray photoelectron spectroscopy (XPS).

2 Experimental

2.1 Syntheses of RTILs and $Dy(TFSA)_3$

P_{2225}TFSA was prepared by the metathesis reaction of P_{2225}Br (Nippon Chemical Industrial Co., Ltd., >99.5 %) with LiTFSA (Kanto Chemical Co., Inc., 99.7 %) according to the reaction process described in a recent paper [14]. The P_{2225}Br was reacted with LiTFSA in distilled water at 70 °C, and then the obtained P_{2225}TFSA was separated into 1,2-dichloroethane (Wako Pure Chemical Industries, Ltd., 99.5 %) by extraction. The separated P_{2225}TFSA was purified by washing it with distilled water several times until no residual halogens were detected by titration with $AgNO_3$ aqueous solution. The extracted 1,2-dichloroethane including P_{2225}TFSA was evaporated at 50 °C for 12 h in a chemical fume hood. Finally, the obtained P_{2225}TFSA was dried in a vacuum chamber at 120 °C for 72 h.

$Dy(TFSA)_3$ was synthesized by reacting Dy_2O_3 (Kanto Chemical Co., Inc., 99.95 %) with HTFSA (Kanto Chemical Co., Inc., 99.0 %) at 150 °C for 20 min under stirring and the reactor vessel was covering with a rigid polymer to prevent the vaporization of the solvent. The obtained products were evaporated at 150 °C for 1 h to remove the unreacted acid components. Finally, the precipitated $Dy(TFSA)_3$ was broken into small pieces and dried in a vacuum chamber at 120 °C for more than 48 h. The average yield of synthesized $Dy(TFSA)_3$ was approximately 98.2 %. A purity of synthesized $Dy(TFSA)_3$ was confirmed by a differential scanning calorimetry (DSC, Rigaku DSC8230) and thermogravimetry differential thermal analysis (TG/DTA, Rigaku TG8120) at a heating rate of 10 °C min^{-1}.

2.2 Solution properties of Dy(III) in RTILs

The dissolution of Dy(III) in various RTILs was confirmed using a UV–Vis–NIR spectrometer (PerkinElmer, Lambda 750) with a quartz microcell (optical path length: 1.0 cm) in the wavelength region of 250–1400 nm. The light sources for the UV and Vis–NIR regions were a deuterium lamp and a halogen lamp, respectively. A cone-plate-type viscometer (Brookfield, LVDV-II+ Pro) was used to measure the temperature dependence of the viscosities of the electrolytic solutions. The water contents of the P_{2225}TFSA samples containing Dy(III) dried at 110 °C under vacuum for 48 h were less than 220 ppm as measured by Karl-Fischer titration (DL32, Mettler-Toledo International Inc.).

2.3 Electrochemical measurements and electrodeposition

CV and SI were carried out at different operating temperatures (50, 60, 75, 90, 100 °C, and 125 ± 1 °C) with an electrochemical analyzer (ALS-910B, BAS Inc.). A platinum electrode with a 1.6-mm inner diameter was used as a working electrode after it was polished with a diamond paste (1 μm) and an alumina paste (0.05 μm). Platinum wires with 0.5-mm inner diameter were employed as counter and quasi-reference electrodes, because the potential obtained using a Pt quasi-reference electrode was stable and exhibited good reproducibility above room-temperature. The P_{2225}TFSA containing $Dy(TFSA)_3$ was used as the electrolytic solution for the CV and SI measurements.

The electrodeposition of Dy was carried out using a cylindrical cell at different operating temperatures (100, 125, 140, and 150 °C). In this study, a dysprosium rod with 6.35-mm inner diameter (Nilaco Corp., >99.5 %) and a copper plate were employed as an anode and a cathode, respectively. The surface of each electrode material was polished by the suitable sandpapers with fine grade. The electrolytic solution was 0.1 M $Dy(TFSA)_3$ in P_{2225}TFSA. The electrodeposits were observed by a scanning electron microscope (SEM, JSM-6510LA, JEOL Ltd.) and analyzed by EDX (JED-2300, JEOL Ltd.). Moreover, the electronic states of the electrodeposits were detected using XPS (Quantera SXM, ULVAC-PHI, Inc.)

3 Results and discussion

3.1 Thermal analysis of $Dy(TFSA)_3$

Thermal analysis such as DSC and TG/DTA provide us a relation between the fusion and decomposition behaviors of the metallic TFSA salts. As shown in Fig. 1, there was only one sharp endothermic peak at 161 °C, which was corresponding to the fusion behavior of $Dy(TFSA)_3$ because there was almost no weight-loss appeared around 160 °C and the enthalpy of fusion, ΔH_f for $Dy(TFSA)_3$ was evaluated to be -35 kJ mol^{-1}, which was very similar to the enthalpy of fusion for pure $Nd(TFSA)_3$ ($\Delta H_f = -38$ kJ mol^{-1}). Above descriptions proved that synthesized $Dy(TFSA)_3$ contained almost no impurities. On the other hand, some complicated peaks appeared around 260 °C on DSC profile and thus thermal behavior was corresponding to the decomposition of $Dy(TFSA)_3$, since the weight-loss was drastically decreased around 260 °C from the result of TG measurement.

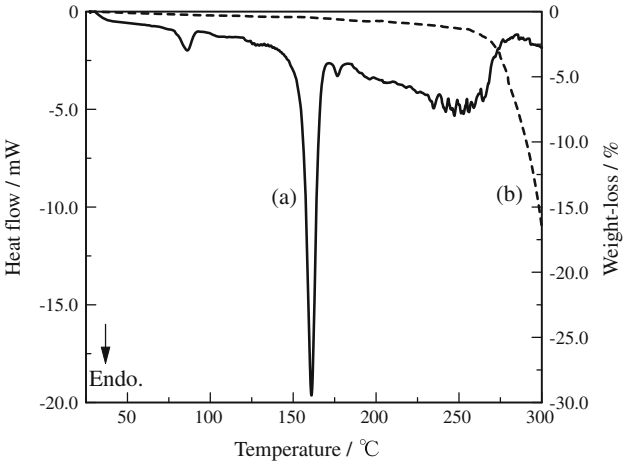

Fig. 1 Thermal analysis results of $Dy(TFSA)_3$ from **a** DSC and **b** TG. A sharp endothermic peak around 160 °C was ascribed to the fusion process of $Dy(TFSA)_3$

3.2 Spectrochemical studies of Dy complexes in RTILs

The UV–Vis–NIR absorption spectra of various ILs (X-TFSA: X = P_{2225}, N_{2225}, or EMI) containing 0.1 M $Dy(TFSA)_3$ shown in Fig. 2 gives evidence for the dissolution of Dy(III) in RTILs. These spectra in Fig. 2 were compensated for the baseline to remove the slight absorption in the UV region related to ILs with no Dy complexes. The UV–Vis absorption spectra of Dy(III) had a narrow and sharp peak ascribed to the f–f transition. The NIR absorption spectra of Dy(III) had broader peaks because of the interaction between the Dy(III) and the surrounding ligands.

The hypersensitive peak of Dy(III) appeared at approximately 1290 nm ($^6H_{15/2} \rightarrow {}^6F_{11/2}$), which is close to the theoretical value [18]. It was reported that the hypersensitive peak was sensitive to the surrounding solvent [19], according to Judd–Ofelt theory [20, 21]. The wavelength was almost constant in different solvents

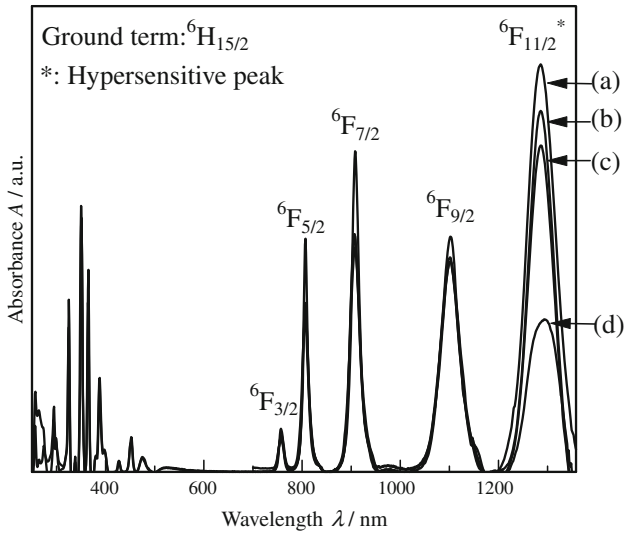

Fig. 2 The UV–Vis–NIR spectra of 0.1 M $Dy(TFSA)_3$ in X-TFSA (X = **a** P_{2225}, **b** EMI, **c** N_{2225}) and **d** distilled water

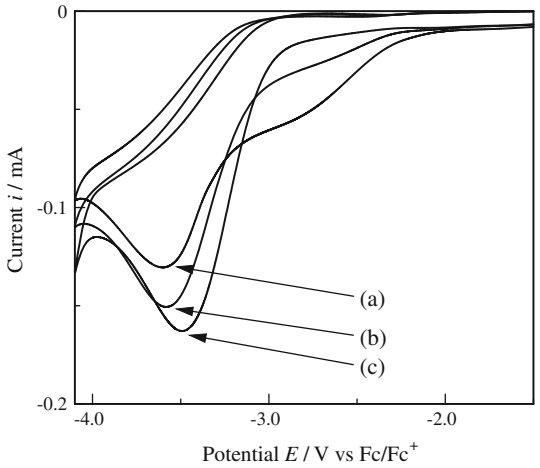

Fig. 3 The reduction peaks from the cyclic voltammograms of 0.075 M $Dy(TFSA)_3$ in $P_{2225}TFSA$ with different scan cycle **a** first, **b** second, and **c** third scan at 90 °C

(various ILs and distilled water). However, the absorbance of the hypersensitive peak was more intense in ILs than in distilled water. The molar extinction coefficients ε of TFSA-based ILs and distilled water containing Dy(III) are tabulated in Table 1 for different wavelengths. The excited state at the maximum molar extinction coefficient ε_{max} in ILs was different from that in distilled water. The transition for ε_{max} of 0.1 M Dy(III)/distilled water was attributed to $^6H_{15/2} \rightarrow {}^6F_{7/2}$. On the other hand, the transition for ε_{max} of 0.1 M Dy(III)/ILs corresponded to $^6H_{15/2} \rightarrow {}^6F_{11/2}$. These results suggest that the solvation structures of the Dy ion were different in aqueous solution and in RTILs. Therefore, to perform a detailed investigation of the coordination structure of Dy(III), Raman spectroscopy should be carried out.

3.3 Cyclic voltammetry of Dy(III) in $P_{2225}TFSA$

Figure 3 shows cyclic voltammograms for 0.075 M Dy(III) in $P_{2225}TFSA$ measured using a Pt electrode at 90 °C. The potential was compensated against the ferrocene/ferrocenium (Fc/Fc^+) redox couple. All cyclic voltammograms in this experiment showed a cathodic peak appearing around −3.5 V. This cathodic peak at around −3.5 V were ascribed to the reduction of Dy(III). As shown in Fig. 3, there is another cathodic peak appearing around −2.7 V for the first and second scan cycles. Moreover, a cathodic peak around −2.7 V grew smaller as the scan cycle proceeded. This cathodic peak around −2.7 V was ascribed to the background current because there were similar reduction peaks appeared for both the $P_{2225}TFSA$ neat solution and $P_{2225}TFSA$ including Dy(III) around −2.7 V in voltammograms. We deduced that this reduction behavior was ascribed to the reduction reaction of trace amount of H_2O containing in RTIL and there was no evidence of reduction behavior for Dy(II) in this ionic liquids. Eventually, the cyclic voltammograms for the third scan had only one cathodic peak around −3.5 V.

Figure 4 shows cyclic voltammograms for the third scan and a plot of the cathodic peak current i_p versus the square root of the scan rate $v^{1/2}$ for 0.075 M Dy(III) in $P_{2225}TFSA$ measured using a Pt electrode at 90 °C with different scan rates. $P_{2225}TFSA$ has a wide electrochemical window at

Table 1 The molar extinction coefficient in 0.1 M Dy(III) in various cation-based IL with TFSA anion

λ_{max}/nm	State	Dy(III) in $P_{2225}TFSA$ ε_1/dm^3 mol^{-1} cm^{-1}	Dy(III) in $N_{2225}TFSA$ ε_2/dm^3 mol^{-1} cm^{-1}	Dy(III) in EMITFSA ε_3/dm^3 mol^{-1} cm^{-1}	Dy(III) in water ε_4/dm^3 mol^{-1} cm^{-1}
756	$^6F_{3/2}$	0.21	0.23	0.25	0.30
807	$^6F_{5/2}$	1.05	1.16	1.11	1.60
908	$^6F_{7/2}$	1.54	1.63	1.62	2.20
1101	$^6F_{9/2}$	1.45	1.47	1.45	1.62
1290	$^6F^*_{11/2}$	2.80	2.24	2.48	1.05

"State" is term symbol of excited state from ground state $^6H_{15/2}$

* Hypersensitive peak

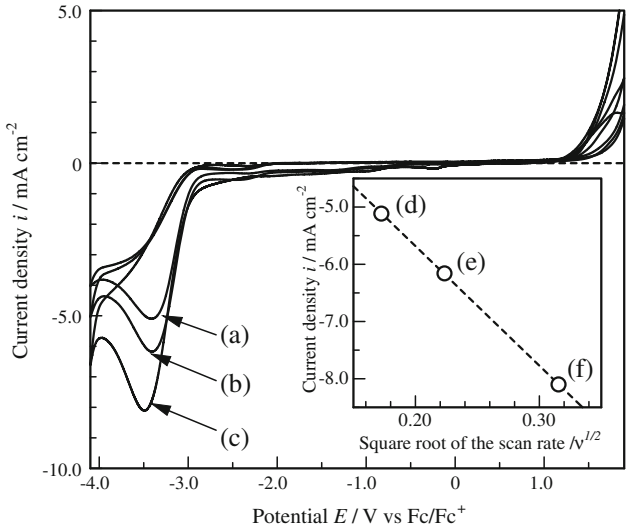

Fig. 4 The cyclic voltammograms of 0.075 M $Dy(TFSA)_3$ in $P_{2225}TFSA$ for 3rd scan with different scan rates **a** 0.03, **b** 0.05 and **c** 0.10 V/s at 90 °C. The interpolated graph showed i_p versus $v^{1/2}$ plot for different scan rate **d** 0.03, **e** 0.05 and **f** 0.10 V/s at 90 °C

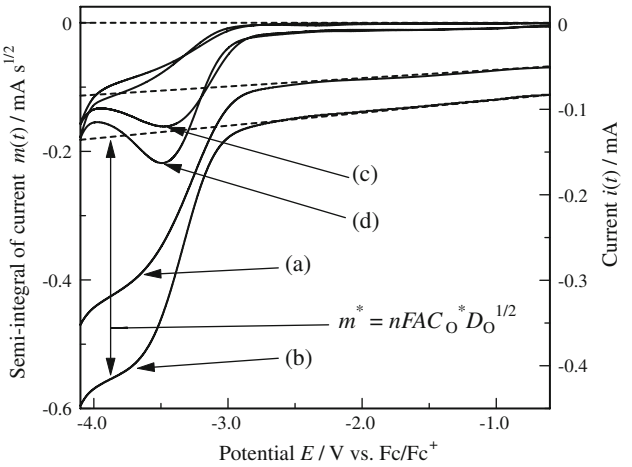

Fig. 5 The semi-integrated curves of 0.075 M $Dy(TFSA)_3$ in $P_{2225}TFSA$ at **a** 60 °C and **b** 90 °C obtained from the 3rd cyclic voltammograms of 0.075 M $Dy(TFSA)_3$ in $P_{2225}TFSA$ at **c** 60 °C and **d** 90 °C with 0.1 V/s

room-temperature (−3.2 to +3.0 V) [13] in the case of using a glassy carbon electrode as a working electrode. The anodic and cathodic limits would be slightly shorter in this study, because the electrochemical window depends on the temperature [22] and the material of the working electrode. Since the reduction potential shifted to a more negative potential as the scan rates became more rapid, the electrochemical behavior of Dy(III) was conjectured to follow an irreversible process. The electrochemical reaction of Dy(III) was also confirmed to be diffusion controlled, because the plot of the peak current against the square root of the scan rate resulted in a straight line. On the other hand, the anodic current appearing around +1.3 V was ascribed to the electrochemically anodic decomposition related with the TFSA anion in $P_{2225}TFSA$. In this experiment, there were no anodic peaks corresponding to an oxidation of Dy(0) at any operating temperature for the various scan rates used in this experiment. Lodermeyer et al. [17] also observed that no dissolution of Dy occurred in dimethylformamide (DMF)/dimethylpyrrolidinium trifluoromethane sulfonate (DMPT). They concluded that no oxidation peak was observed because of the irreversible plating process. The CV results in this study also suggest an irreversible system.

3.4 Semi-integral analysis and diffusion coefficients

SI enabled us to evaluate the diffusion coefficient of Dy(III) more accurately by analyzing the SI limiting current m^*. From the cyclic voltammograms of 0.075 M Dy(III)/Dy in $P_{2225}TFSA$ measured using a Pt electrode at 60, 90, and 100 °C, the SI curves were obtained by convolution analysis, as shown in Fig. 5. The values of m^* were determined by subtracting the background current illustrated as broken line from the flat part of SI curve corresponding to reduction of Dy(III). The D_O values of Dy(III) were calculated from the estimation of the SI limiting current according to the following equation [23]:

$$m^* = nFAC_O^* D_O^{1/2} \quad (1)$$

where n is the number of electrons involved in the charge transfer reaction, F is the Faraday constant, A is the electrode surface area, and C_O^* is the bulk concentration of the electroactive species. In RTILs, the diffusion coefficient of the metal complexes is generally influenced by the electrostatic interaction and depends on the electric charge of the central metal [7]. Thus, it is important to investigate the diffusion properties of the trivalent complex in RTILs for comparison with those of the divalent complex. The diffusion coefficient of the trivalent Dy complex (Dy(III)) was calculated to be 2.0×10^{-12} m^2 s^{-1} at 25 °C. This value is in good agreement with those of the trivalent rare-earth complexes of Eu(III) and Sm(III) [7] listed in Table 2.

3.5 Activation energy for diffusion

In general, the mobility of cations in the electrolytic solution is influenced by the electrostatic attraction involved in the formation of the metal complexes. Thus, it is anticipated that the cations in ILs will diffuse when their energy exceeds the dissociation energy required to separate them from the surrounding anions in the metal complexes. Therefore, we investigated the activation energy for diffusion $E_{a,D}$ of the Dy complexes (Dy(III)) in $P_{2225}TFSA$.

Table 2 The diffusion coefficient D of some trivalent rare-earth complexes in P_{2225}TFSA at 25 °C

Ionic species	Methods	$D/10^{-12}$ m^2 s^{-1}	Reference
Dy(III)	SI	2.0	This work
Eu(III)	CA	2.6	[7]
	CP	2.4	[7]
Sm(III)	CA	2.8	[7]
	CP	2.4	[7]

CA Chronoamperometry, *CP* Chronopotentiometry

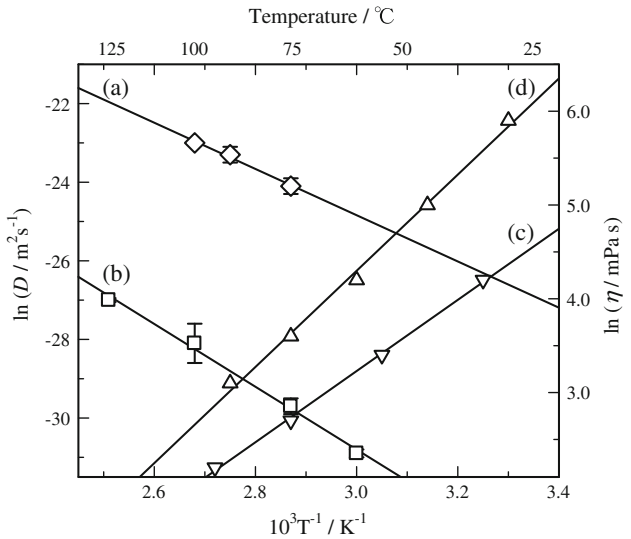

Fig. 6 The Arrhenius plots of 0.075 M Dy(III) in P_{2225}TFSA from **a** diffusion coefficient and **b** viscosity in comparison with that of 0.5 M Dy(III) in P_{2225}TFSA from **c** diffusion coefficients and **d** viscosity

The $E_{a,D}$ value was controlled by the Arrhenius rule, which is given by the following equation:

$$D = A_{exp}\,(-E_{a,D}/RT) \quad (2)$$

where A is the frequency factor, which is not related to the activation energy, R is the gas constant, and T is the absolute temperature. A logarithmic plot of the diffusion coefficient for Dy(III) against the inverse of the temperature is given in Fig. 6. The given errors were evaluated from the measurement results obtained from the different scans. The logarithmic value of the diffusion coefficient for Dy(III) in Fig. 6 increased with increasing temperature. The rate of increase for 0.5 M Dy(III) in P_{2225}TFSA was larger than that for P_{2225}TFSA with 0.075 M Dy(III). From the above Eq. 2, the $E_{a,D}$ values for 0.075 M and 0.5 M Dy(III) in P_{2225}TFSA calculated by SI were determined to be 49 and 65 kJ mol^{-1}, respectively.

The activation energy for diffusion of Dy(III) in the phosphonium-based IL was also dependent on the concentration and the viscosity of the bulk solution. Figure 6

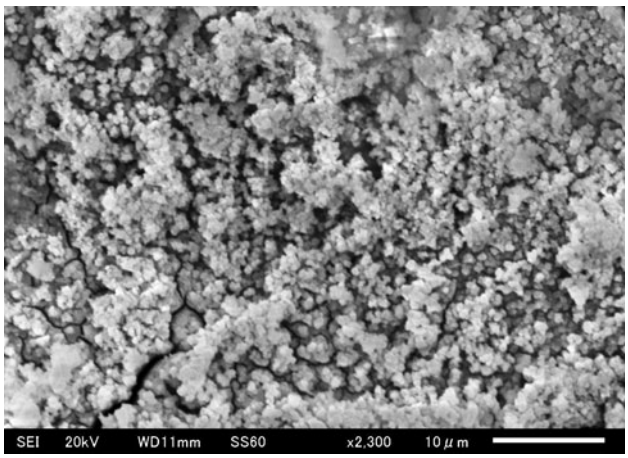

Fig. 7 The SEM image of the electrodeposits on a Cu substrate in 0.1 M Dy(III)/P_{2225}TFSA with −3.8 V at 150 °C

shows that the apparent activation energy values $E_{a,\eta}$ estimated from the viscosities by the Andrade formula ($\eta = A_{exp}\ (E_{a,\eta}/RT)$) [24] were determined to be 43 kJ mol^{-1} (0.5 M), 34 kJ mol^{-1} (0.1 M), and 33 kJ mol^{-1} (0.075 M). The above results demonstrate that the apparent activation energy of phosphonium-cation-based ILs containing Dy(III) calculated from the viscosity depend on the concentration of Dy(III) in the IL, because the electrostatic attraction between the Dy(III) cation and TFSA anion is affected by the concentration in this concentration range. These series of experimental results suggest that Dy metal can be effectively recovered by electrowinning in RTILs based on phosphonium cations when the operating temperature and the concentration of the electrolytic solution are controlled.

3.6 Electrodeposition of Dy metal

Electrodeposition of Dy metal from 0.1 M Dy(III) in P_{2225}TFSA at 150 °C was performed by a two-electrode system. We defined "induced potential" as the total voltage considering from both the bulk resistance and the metal/IL interfacial resistance during potentiostatic electrolysis. Thus induced potential and the cathodic current density were −3.8 V and −3.2 mA cm^{-2} during the potentiostatic electrodeposition, respectively. The electrolytic solution was clear pale yellow before the electrodeposition; however, this electrolytic solution turned clear brownish yellow after the electrodeposition. SEM images of the gray electrodeposits obtained at −3.8 V with a current density of −1 to −2 mA cm^{-2} are shown in Fig. 7. The surface morphology was granular with cracks, and the particle diameter was approximately 0.5 μm. Each cathodic and anodic current efficiency was estimated from the respective mass change. The weight of copper plate which was employed as a cathodic material increased as the electrodeposition

proceed. On the other hand, the weight of Dy rod which was employed as an anodic material decreased since Dy(0) oxidized to Dy(III). The cathodic and anodic current efficiencies of the electrodeposition at −3.2 V in the temperature range from 100 to 140 °C were 74.5 ± 2.5 and 77.5 ± 7.5 %, respectively. The loss of current efficiency would be due to the decomposition of the electrolytic solution.

Figure 8 shows the EDX spectra of the electrodeposits formed at −3.2 V for a total transported charge of 35 C at 100 and 125 °C. The increase in the relative abundance of Dy in the electrodeposit arose from the electrolytic temperature, since the reduction potential of Dy was shifted positive by the elevated temperature. Although a large Dy peak was observed by EDX, there was no evidence that the obtained Dy was in a metallic state in this spectrum. The relatively large oxygen peak would suggest that part of the surface layer of the electrodeposit was a Dy oxide layer since the electrodeposition was performed not under argon saturated but under atmosphere condition. To determine the electronic state of the obtained Dy, XPS was performed with Al Kα radiation. It is known that the Dy $3d_{5/2}$ peak has a somewhat high photoionization cross section [25]. The XPS spectrum in Fig. 9 shows that the Dy $3d_{5/2}$ peak was at a higher binding energy than the theoretical peaks for Dy metal and Dy_2O_3. Theoretically, the Dy $3d_{5/2}$ peaks for metallic Dy and Dy oxides are at 1295.8 and 1289.0 eV, respectively [26]. In order to remove the oxidized layer on the electrodeposit surface, it was etched with argon plasma, as shown in Fig. 9b and c. After the argon etching, the observed Dy $3d_{5/2}$ peak shifted to a lower binding energy in good agreement with the theoretical Dy metal value. These results reveal that there were no Dy oxides in the obtained electrodeposits other than the surface layer. The inconsistency of the two X-ray analyses, i.e., EDX and XPS, can be explained as follows: the surface layer of the electrodeposits was partially nonmetallic, and the inner parts of the electrodeposits were Dy metal.

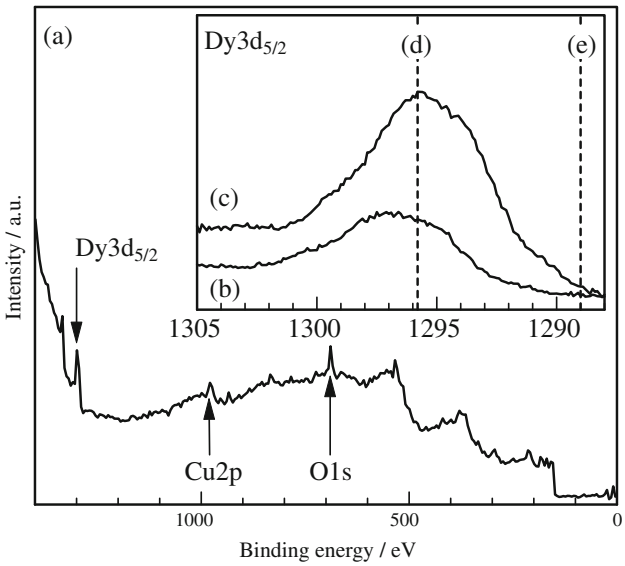

Fig. 9 **a** The survey XPS spectrum of the electrodeposits at 140 °C with −3.2 V. To remove the affect from the oxidation for the surface layer of Dy, The $Dy3d_{5/2}$ peaks were measured after the Ar etching approximately by **b** 28 nm and **c** 280 nm. The theoretical binding energy of $Dy3d_{5/2}$ for Dy metal and Dy_2O_3 was 1295.8 eV (a broken line (**d**)) and 1289.0 eV (a broken line (**e**)), respectively

4 Conclusions

In this study, we focused on the electrochemical and diffusion properties of Dy complexes in phosphonium-based ILs. Moreover, the electrodeposition of Dy metal in this IL was investigated. For this purpose, the electrochemical behaviors of Dy(III) in phosphonium-based IL were measured by

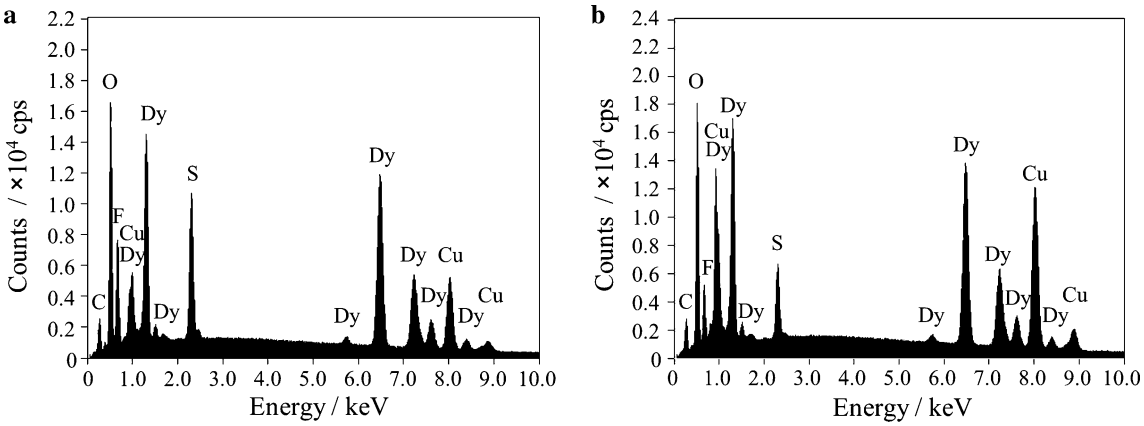

Fig. 8 The EDX spectra of the electrodeposits with −3.2 V for 35 C at **a** 100 °C, **b** 125 °C showed that the dysprosium characteristic X-ray increased as elevating temperature, since the reduction potential was shifted positively with elevating temperature

CV and SI. The CV results indicated that the reduction process of Dy(III) had one step: $Dy(III) + 3e^- \rightleftharpoons Dy(0)$. A series of experimental results indicated that the electrochemical behavior of the trivalent Dy complex was similar to that of other lanthanoid complexes such as europium and samarium complexes. The diffusion coefficient estimated from SI of 0.075 M Dy(III) was on the order of 2.0×10^{-12} m^2 s^{-1} at 25 °C, and the activation energy for diffusion was evaluated to be 49 kJ mol^{-1}. Electrodeposition was carried out at different potentials (−3.2 and −3.8 V), and the average cathodic efficiency was calculated to be 74.5 ± 2.5 %. The obtained electrodeposits were metallic Dy, as identified by XPS, and the surface layer of the electrodeposits was partially oxidized, as shown in the EDX spectrum. Further investigations are needed to clarify the electrodeposition process of Dy in phosphonium-cation-based ILs.

Acknowledgments This study was partially supported by the research grant program on the Promotion of a Recycle-Based Society in 2010 from the Ministry of the Environment, Japan.

References

1. Kim CH, Kwon IE, Park CH, Hwang YJ, Bae HS, Yu BY, Pyun CH, Hong GY (2000) J Alloys Compd 33:311
2. Ryunhong G, Miura N, Matsumoto H, Nakano R (2006) J Rare Earths 24:119
3. Oono N, Sagawa M, Kasada R, Matsui H, Kimura A (2011) J Magn Magn Mater 323:297
4. Miura K, Itoh M, Machida K (2008) J Alloys Compd 466:228
5. Matsuura Y (2006) J Magn Magn Mater 303:344
6. Zhu YL, Kozuma Y, Katayama Y, Miura T (2009) Electrochim Acta 54:7502
7. Matsumiya M, Suda S, Tsunashima K, Sugiya M, Kishioka S, Matsuura H (2008) J Electroanal Chem 622:129
8. Vega JA, Zhou J, Kohl PA (2009) J Electrochem Soc 156(4):A253
9. Fukui R, Katayama Y, Miura T (2011) Electrochim Acta 56:190
10. Komaba S, Yabuushi N, Ozeki T, Okushi K, Yui H, Konno K, Katayama Y, Miura T (2010) J Power Sources 195:6069
11. Orita A, Kamijima K, Yoshida M, Dokko K, Watanabe M (2010) J Power Sources 196:3874
12. MacFarlane DR, Meakin P, Shn J, Amini N, Forsyth M (1999) J Phys Chem B 103:4164
13. Tsunashima K, Sugiya M (2007) Electrochem Commun 9:2354
14. Tsunashima K, Sugiya M (2007) Electrochemistry 75(9):734
15. Saïla A, Gibilaro M, Massot L, Chamelot P, Taxil P, Affoune AM (2010) J Electroanal Chem 642:150
16. Castrillejo Y, Bermejo MR, Barrado AI, Pardo R, Barrado E, Martínez AM (2005) Electrochim Acta 50:2047
17. Lodermeyer J, Multerer M, Zistler M, Jordan S, Gores HJ, Kipferl W, Diaconu E, Sperl M, Bayreuther G (2006) J Electrochem Soc 153:C242
18. Tachikawa N, Katayama Y, Miura T (2007) J Electrochem Soc 154(11):F211
19. Katayama Y, Miura T (2010) Electrochemistry 78(10):808
20. Fujii K, Nonaka T, Akimoto Y, Umebayashi Y, Ishigro S (2008) Anal Sci 24:1377
21. Zhu YL, Katayama Y, Miura T (2010) Electrochim Acta 55:9019
22. O'Mahony AM, Silvester DS, Aldous L, Hardacre C, Compton RG (2008) J Chem Eng Data 53:2884
23. Bard AJ, Faulkner LR (2001) Electrochemical methods, fundamentals and applications. John Wiley & Sons, New York, p 248
24. Andrade EN, Chiong YS (1936) Proc Phys 48:247
25. Moslemzadeh N, Barrett SD (2002) J Electron Spectrosc Relat Phenom 127:161
26. Handbook of X-ray photoelectron spectroscopy, ULVAC-PHI Inc